Insular Cortex Mediates Attentional Capture by Behaviorally Relevant Stimuli after Damage to the Right Temporoparietal Junction

Ptak, Radek; Pedrazzini, Elena

How to cite

PTAK, Radek, PEDRAZZINI, Elena. Insular Cortex Mediates Attentional Capture by Behaviorally Relevant Stimuli after Damage to the Right Temporoparietal Junction. In: Cerebral Cortex, 2021. doi: 10.1093/cercor/bhab082

This publication URL: https://archive-ouverte.unige.ch/unige:151408
Publication DOI: 10.1093/cercor/bhab082

Insular cortex mediates attentional capture by behaviorally relevant stimuli after damage to the right temporo-parietal junction

Abbreviated title: Insular cortex mediates attentional capture

Manuscript accepted for publication in Cerebral Cortex (doi: 10.1093/cercor/bhab082)

Radek Ptak[1,2] and Elena Pedrazzini[3]

[1]*Laboratory of Cognitive Neurorehabilitation, Department of Clinical Neurosciences, Faculty of Medicine, University of Geneva, 1206 Geneva, Switzerland*

[2]*Division of Neurorehabilitation, University Hospitals of Geneva, 1206 Geneva, Switzerland*

[3]*Division of Neurology, University Hospitals of Geneva, 1206 Geneva, Switzerland*

Correspondence:

Radek Ptak, PhD; radek.ptak@hcuge.ch

Division of Neurorehabilitation

Department of Clinical Neurosciences

Geneva University Hospital

26, Av. de Beau-Séjour

1206 Geneva

Switzerland

Tel.: +41-22/372 35 24

Conflict of interest: The authors declare no competing financial interests.

Acknowledgement: Study supported by the Swiss National Science Foundation (grant 32003B-184702) and the Novartis Foundation for medical-biological Research (grant 16C183).

Abstract

The right temporo-parietal junction (rTPJ) and insula both play a key role for the processing of relevant stimuli. However, while both have been conceived as neural 'switches' that detect salient events and redirect the focus of attention, it remains unclear how these brain regions interact to achieve this behavioral goal. Here, we tested human participants with focal left-hemispheric or right-hemispheric lesions in a spatial cuing task that requires participants to react to lateralized stimuli preceded by a distracter that shares or does not share a relevant feature with the target. Using machine learning to identify significant lesion-behavior relationships we found that rTPJ damage produces distinctive, pathologically increased attentional capture, but only by relevant distracters. Functional connectivity analyses revealed that the degree of capture is positively associated with a functional connection between insula and rTPJ, together with functional isolation of the rTPJ from right dorsal prefrontal cortex (dPFC). These findings suggest a mechanistic model where the insula-rTPJ connection constitutes a crucial functional unit that breaks attentional focus upon detection of behaviorally relevant events, while the dPFC appears to attune this activity.

Keywords: functional connectivity; spatial attention; relevance; temporo-parietal junction; attention network, insula.

Introduction

Humans may orient attention toward various stimuli and sensations, including individual objects, salient features, social or emotional cues or time intervals (Egeth and Yantis 1997; Coull and Nobre 1998; Simons 2000; Theeuwes 2010; Ptak 2012). This ubiquity of spatial attention has been related to the interplay between controlled (or, goal-driven) and reflexive (or, stimulus-driven) processes (Cave and Bichot 1999; Itti and Koch 2001; Baluch and Itti 2011; Gilbert and Li 2013). The former come into play when observers focus deliberately on particular items or spatial locations, while the latter reflect the capture of attention by suddenly appearing or physically salient stimuli. Distinct functional networks activate when participants orient their attention toward stimuli in their visual periphery, including dorsal parietal, premotor and prefrontal cortex, as well as the right temporo-parietal junction (rTPJ) and insular cortex (Kincade et al. 2005; Serences et al. 2005; Indovina and Macaluso 2007; Szczepanski et al. 2010). An influential hypothesis posits that target detection and goal-directed orienting rely on a bilateral dorsal network, while the rTPJ is crucial for reorienting toward salient, unexpected or infrequent distracters (Corbetta and Shulman 2002; Shulman et al. 2009). This proposal fits with the finding that damage to the rTPJ impairs contralateral reorienting following attentional engagement in the right hemifield, an effect known as the disengagement deficit (Posner et al. 1984; Friedrich et al. 1998). Together, functional imaging and lesion studies indicate that distracter effects at the rTPJ are due to stimulus-driven mechanisms, and that any salient stimulus potentially interrupts and impairs reorienting of attention.

However, a weakness of the controlled – reflexive dichotomy is that motivational components of actions sometimes influence attention implicitly rather than through controlled mechanisms (Awh et al. 2012). An example is the effect of selection history, where previous targets continue to capture attention even after their status has switched to distracter (Maljkovic and Nakayama 1994). Counterintuitively, motivational values may also operate outside of consciousness, as stimuli or positions in space associated with reward may capture attention though they are entirely irrelevant for the current task (Anderson et al. 2011; Chelazzi et al. 2014). Goal-directed processing may even decrease task performance, such as when stimuli sharing relevant features with the target distract attention from the current task (Folk et al. 1992; Eimer and Kiss 2008). A question emerging from these findings is whether computations of a stimulus' behavioral relevance occur within or outside the attention networks. Previous studies have shown that distracters sharing relevant features with the target have privileged access to working memory (Knudsen 2007; Baluch and Itti 2011) because these features are automatically linked to a behavioral response. This makes the dorsal prefrontal cortex (dPFC), whose activity correlates with the maintenance and manipulation of contents in working memory, the presumed source of top-down modulation of attention networks (Knudsen 2007; Ptak 2012). Alternatively, feature relevance may be processed by the saliency network, which comprehends the anterior cingulate gyrus, insular cortex (IC) and amygdala, and is activated by salient external stimuli and bodily sensations (Seeley et al. 2007). The anterior IC in particular is believed to interact with attention networks by facilitating processing of salient and biologically relevant information (Menon and Uddin 2010; Uddin 2015).

Here, we tested these different proposals by evaluating to what extent relevant and irrelevant distracters capture attention of patients with focal left (LH) or right hemisphere (RH) damage that were sampled without anatomical selection criteria. We then applied machine learning techniques to identify regions in the injured brain that are crucial for the orienting and capture of attention. We then assessed functional connectivity (FC) at rest and examined functional interconnections between distant brain regions that may predict capture of attention. Our results confirm that damage to the rTPJ leads to a disengagement deficit, but challenge previous studies, in that we report that this effect is highly specific to relevant cues. Crucially, we show that functional interactions between the insula, dPFC and rTPJ predict the pathological capture of attention by behaviorally relevant stimuli.

Methods

Participants. Approval for this study was obtained from the local ethical committee (Geneva, Switzerland), and all participants gave written informed consent before being enrolled. The study was performed on three samples recruited for the behavioral study and one sample providing control data for the resting-state (rs) fMRI study. The first two samples consisted of 71 patients with right-hemisphere (RH) and 12 patients with left-hemisphere (LH) stroke hospitalized for rehabilitation at the Division of neurorehabilitation, University Hospitals Geneva. Inclusion criterion was a first-ever hemispheric stroke that was clearly identifiable with MRI or computer tomography (CT). Exclusion criteria were a) presence of prior strokes or multiple lacunar lesions, b) severe cognitive impairment precluding administration or interpretation of clinical tests (e.g., severe hypovigilance or confusion) and c) presence of other neurological or severe psychiatric diseases. An additional exclusion criterion for LH patients was the presence of aphasia (though slight language problems such as anomia were permitted). Importantly, in order to obtain unbiased samples, no a priori anatomical criteria were applied. Moreover, the main focus of our study was on right-hemispheric attention networks, and LH patients were merely included to test whether the spatial attention variables studied were similarly vulnerable to RH and LH damage. Therefore, we did not seek to obtain entirely comparable samples and accepted that the exclusion of aphasic patients possibly biased the LH-sample toward more posterior lesions. All patients were studied in a sub-acute stage of disease. Sample 3

consisted of 12 healthy control participants who performed only the behavioral task. The fourth sample was composed of 27 healthy subjects who provided rs-fMRI data acquired in a previous study (Goveas et al. 2013; data freely available through the 1000 Functional Connectomes Project at http://fcon_1000.project.nitrc.org).

Table 1 provides demographic characteristics of all samples and the test results of the two patient samples. Given the focus of this study, the clinical examination particularly payed attention to deficits in the spatial domain. All patients had a neuropsychological examination including visual field testing through digital confrontation, and were administered a symbol cancellation test (Gauthier et al. 1989), letter cancellation (Ptak et al. 2007), line bisection (Ronchi et al. 2012), word reading (Ptak et al. 2012) and clock drawing (Royall et al. 1998).

Spatial attention task. A spatial cuing task with different types of cues was employed to test participants' speed of orienting toward a target following a peripheral cue (Pedrazzini and Ptak 2019). All stimuli were composed of two 1° × 3° bars presented in a parallel (cues; horizontal bars separated by 4.5°) or perpendicular arrangement (targets and distracters; bars forming an L- or T-shape, presented at orientations 0°, 90°, 180° or 270°; Fig. 1a). Stimuli were pale red (RGB-values: 222, 80, 80), green (0, 180, 0) or blue (10, 150, 250). These RGB-values had the same luminance in our experimental setup (25 cd/m^2), but were slightly brighter than the gray background (15 cd/m^2).

Table 1. Demographic characteristics of the four samples (mean ± SEM).

		Sample			
		RH-damaged	LH-damaged	Experimental control	fMRI control
Sex	female / male	28 / 43	4 / 8	8 / 4	12 / 15
Age	years	61.84 ± 1.60	64.48 ± 3.25	54.7 ± 3.0	55.9 ± 6.1
Time post stroke	days	53.93 ± 4.74	65.58 ± 19.56	-	-
Time post imaging	days	34.76 ± 6.77	19.17 ± 10.51	-	-
Lesion volume	cm^3	82.12 ± 10.20	43.59 ± 9.03	-	-
Handedness	right / left	66 / 5	11 / 1	12 / 0	-
Hemiparesis	yes / no	52 / 19	8 / 4	-	-
Visual field	preserved / impaired	53 / 18	9 / 3	-	-
Bells cancellation	left omissions (max. 15)	4.94 ± .62	1.42 ± .58	-	-
	right omissions (max. 15)	2.06 ± .33	1.75 ± .82	-	-
Letter cancellation	left omissions (max. 27)	7.10 ± 1.03	0.33 ± .14	-	-
	right omissions (max. 27)	3.35 ± .55	1.00 ± .49	-	-
Line bisection	bias, %	3.57 ± .61	-1.71 ± .73	-	-
Reading	omissions (max. 40)	6.57 ± 1.04	2.67 ± 1.34	-	-
Clock drawing	points (max. 10)	7.63 ± .33	7.58 ± .71	-	-

Participants sat at ~60 cm distance from a 21-inch screen. At the beginning of the testing session one color was randomly selected as the target color and would remain the same throughout testing. The sequence of events during a trial is shown in Fig. 1b. Participants were instructed to press the space bar upon presentation of an L- or T-shape in their respective target color (go trial) and to withhold reaction if this color was not present (no-go trial). In each trial a single cue was first shown 5° left or right of fixation, followed by a target display always containing two colored shapes (either a target and a distracter or two distracters). One of the two shapes appeared at the position previously occupied by the cue and the other at a mirror position in the opposite visual field. Cues were valid if they appeared at the same position as the upcoming target, and relevant if they had the target color (Fig. 1c). The experimental design had thus four factors: target position (left, right), cue validity (valid, invalid), cue relevance (relevant or irrelevant) and ISI (100 ms, 600 ms). Conditions were orthogonally varied in blocks of 96 trials containing 64 go and 32 no-go trials. Every participant performed eight blocks, resulting in 32 reactions for each condition.

Given that no action was required to the cues and the presence of a target was independent of the presence of a particular cue, any effects of cues on performance were due to involuntary processes. Capture of attention was operationalized as the slowing of reaction times (RTs) following an invalid cue as compared to a valid cue.

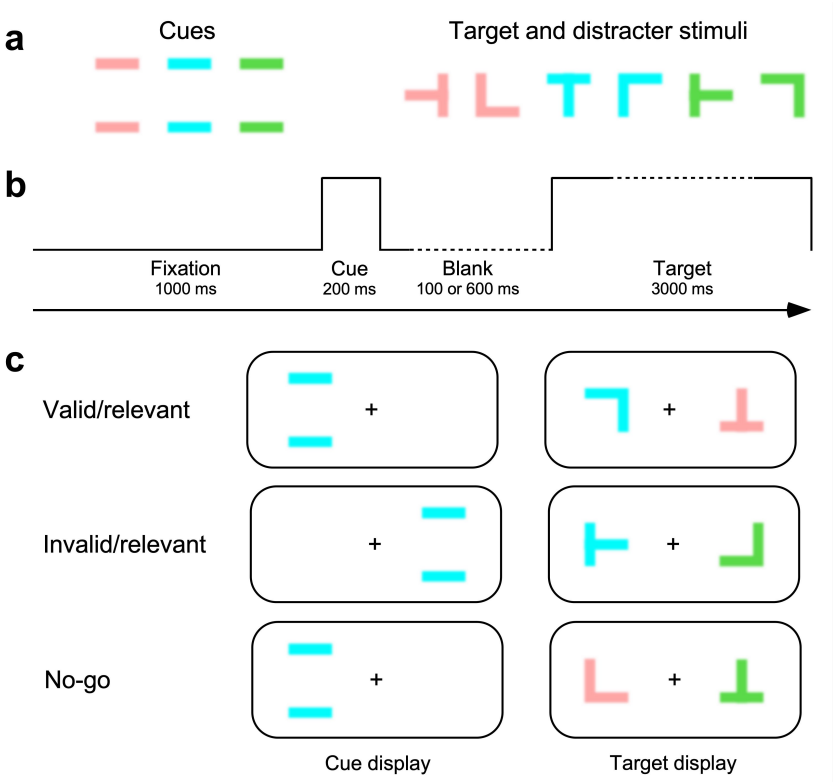

Fig. 1. Stimuli and behavioral task design. a, The three types of cues and a selection of possible target/distracter stimuli. For each color there were eight T- and L-stimuli, for a total of 24 different items. **b**, Time-course of a single trial. **c**, Examples of cue-target combinations. In the example shown here (the target color is blue) participants have to press the space bar if either stimulus of the target display is blue (go trial), and to withhold reaction otherwise (no-go trial). Valid/invalid and relevant/irrelevant cues are equally likely, hence the occurrence or absence of a target cannot be predicted from the presence of a particular cue.

Structural MRI acquisition and preprocessing. Of the 71 right-hemisphere damaged stroke patients, 44 had a low-resolution (clinical) MRI (N = 41) or a CT (N = 3) scan and 27 participated to an fMRI session which included high-resolution structural scans. All LH-damaged patients had a low-resolution MRI scan. MRI scans were acquired on a 3T Trio scanner (Siemens Medical Solutions, Erlangen, Germany) in a single session. Low-resolution MRI imaging included axial FLAIR, T1- and T2-weighted sequences with a slice resolution of 4 mm^3. High-resolution images had a voxel size of 1 mm^3 and consisted of a T1-weighted MPRAGE sequence (TR: 2300 ms; TE: 1.94 ms; flip angle 9°) and a T2-weighted (TR: 3200 ms; TE: 407 ms; flip angle 120°) structural scan.

For each patient the lesion was delineated with a graphic tablet directly on the T2-weighted MRI scan using MRIcron software (Rorden et al. 2007). The binary lesion mask thus obtained and the T2-scan were coregistered with the structural T1 using SPM12 (www.fil.ion.ucl.ac.uk/spm). The structural T1-scan was then segmented and normalized to the Montreal Neurological Institute (MNI; http://www.bic.mni.mcgill.ca) template space (voxel size: 2 mm^3) and the normalization parameters were applied to the lesion mask. These steps were performed with the Clinical Toolbox (Rorden et al. 2012), which offers an age-specific MRI template and automatically applies an enantiomorphic lesion mask to minimize normalization artifacts induced by abnormal tissue (Nachev et al. 2008). The same toolbox was used to normalize CT scans.

Lesion-symptom mapping. Lesion-symptom mapping (LSM) was performed by applying support vector regression (SVR) with a Gaussian kernel to the 71 RH lesion masks (Zhang et al. 2014). SVR-LSM is a multivariate approach that has several advantages over classic mass-univariate methods. Mass-univariate LSM examines the relationship between brain damage and behavioral variables in a voxel-wise manner, where each voxel is assumed to be statistically independent from its neighbors. However, since the distribution of stroke lesions depends on anatomical factors such as brain vascularization, damage is not random, and consequently

lesions to neighboring voxels are strongly correlated. Previous studies have shown that mass-univariate approaches may mislocalize the 'true' damage, particularly when lesions cluster around areas of vascular vulnerability (Mah et al. 2014; Sperber and Karnath 2018; Sperber et al. 2019). In addition, by considering voxels as independent, mass-univariate methods cannot take advantage of correlations between neighboring voxels to increase statistical power (Ghaleh et al. 2020). An additional problem these methods struggle with is the correction of confounds such as lesion volume, which is generally a strong, yet unspecific predictor of behavioral scores.

SVR-LSM is a machine-learning classification method which transforms input data (voxels) into a high-dimensional feature space and seeks to apply a multiple regression model that best predicts continuous behavioral data (Zhang et al. 2014). Since the number of predictors (lesioned voxels) is much greater than the number of subjects, a multiple-regression model of the data is severely under-determined and may potentially give an infinite number of solutions. This problem is solved by constraining the fitting coefficients in the feature space, and the trade-off between this constraint and the fitting error is controlled by adjusting the parameter C (or cost) of the model. An additional parameter γ defines the width of the Gaussian kernel. The boundary (or hyperplane) thus identified can be projected (i.e., inverse transformed) back into the original data space. This back-projection creates a voxelwise β-map that can then be tested against alternative solutions to identify the best anatomical predictor of the behavior of interest.

We used a recently developed SVR-LSM toolbox (DeMarco and Turkeltaub 2018) to examine the relationship between regional damage and behavioral scores derived from the experimental testing. We used model parameters C = 30 and γ = 5, which were previously found to be optimal for reproducibility and prediction accuracy (Zhang et al. 2014). Behavioral data were reduced to derive three meaningful indices that could be used as predicted observations in the SVR-LSM analysis: the hemifield effect, the validity effect and the relevance effect. The hemifield effect (computed as the difference between RTs to all LVF targets vs. all RVF targets) reflected general distribution of RTs across both hemifields. The validity effect (difference between RTs to LVF targets after invalid cues vs. valid cues) was a measure of the cost of target processing that was due to cue validity. The relevance effect (difference between RTs to LVF targets after invalid/relevant cues vs. invalid/irrelevant cues) reflected the increased cost of invalid cuing that was due specifically to the behavioral relevance of the cue.

Since the sensitivity of lesion-symptom studies is affected by the minimal number of participants sharing damage to a specific area (Sperber and Karnath 2017), SVR-LSM models were only applied to voxels that were damaged in a minimum of five participants. To control for lesion size lesion volume was regressed out of the lesion data and the behavioral scores at the voxel level. The β-values were tested voxel-wise at $p < .005$ and cluster-wise at $p < .05$ against a permutation-derived distribution (N = 5000 permutations) of random behavioral scores.

Functional MRI acquisition and processing. 27 patients with focal right-hemisphere damage participated to a rs-fMRI examination. The resting-state sequence consisted of 320 volumes acquired using T2*-weighted GRE echo-planar imaging (EPI) sequence (TR: 1500 ms; TE: 35 ms; voxel size 3 x 3 x 5 mm; flip angle 85°). During acquisition each subject's head was fixed with cushions to prevent motion, and participants lay in the dark, eyes closed. Control data were acquired on a 3T Sigma GE scanner (GE Healthcare Technologies, Waukesha, Wisconsin) and consisted of a high-resolution (voxel size: 1 mm^3) 3D spoiled gradient-recalled echo anatomical scan (TR: 10 ms; TE: 4 ms; flip angle 12°) and 175 volumes EPI-sequence (TR: 2000 ms; TE: 25 ms; voxel size 3.75 x 3.75 x 4 mm; flip angle 90°).

The CONN toolbox (Whitfield-Gabrieli and Nieto-Castanon 2012) was used for the preprocessing of control's structural and functional images (including segmentation of the structural T1 and normalization to MNI). Normalized images (including patients' MRIs that had been preprocessed with the Clinical toolbox were smoothed with an 8 mm FWHM function. Outlier scans were identified with an ART-based scrubbing procedure (Power et al. 2012; Caballero-Gaudes and Reynolds 2017), and artefacts from physiological nuisance factors or movement with corrected with a linear regression model with the following variables: a) the six rigid-body parameters estimated from realignment, b) averaged BOLD signals of white matter and cerebrospinal fluid and c) the scrubbing parameters. Finally, the data were filtered with a band-pass of 0.008-0.09 Hz to remove low-frequency drift and high-frequency noise. Controls had on average 0.25% outlier scans identified by scrubbing and a maximum framewise displacement < 0.5 mm. One patient had an excessive number of outlier scans (> 15%) and was therefore eliminated from further analysis. The remaining 26 patients had on average 1.8% outlier scans and a maximum framewise displacement < 0.5 mm.

We used the Harvard-Oxford atlas of cortical regions (Desikan et al. 2006) to define 51 regions of interest (ROIs) in each hemisphere as cortical seeds of functional connectivity (FC). In order to limit the number of comparisons we excluded from the analysis the cerebellum, brain-stem and midline ROIs that cover areas of both hemispheres. FC was quantified as Fisher-transformed bivariate correlation coefficients between each seed-ROI and all voxels of the brain. Family-wise error was controlled by applying a voxel-wise statistical threshold of p <

.001 (uncorrected) for the initial definition of clusters of interest, followed by cluster-level inference testing using Gaussian Random Field theory (computation of the probability at p < .05 to observe a cluster of equal size under the null hypothesis). We additionally computed ROI-to-ROI connectivity between ROIs identified as significant predictors of behavior in the seed-to-voxel analysis (insular cortex, amygdala and dPFC) and five ROIs of the right-hemispheric attention network: middle (mPFC) and ventral PFC (vPFC), angular gyrus (Ang), anterior (aSMG) and posterior supramarginal gyrus (pSMG). ROI-to-ROI connections were tested with t-tests whose significance level was adapted with a false discovery rate (FDR) correction for the total number of connections examined within this mini-network (N = 28). In order to control for confounds created by the lesion all analyses included lesion volume as additional regressor in second-level connectivity analyses (Ptak et al. 2020).

Results

Behavioral data. Repeated-measures analyses of variance (ANOVA) with the factors target position, validity and relevance were performed for each group and ISI. Healthy participants showed no main effect or interaction at ISI100, but a significant effect of target position at ISI600 ($F_{1,11}$ = 6.65, P = .026, η^2 = .377), with slower RTs to left than right hemifield targets (443.4 vs 432.9 ms; Fig. 2a). In addition, there was a significant effect of validity ($F_{1,11}$ = 10.99, P = .007, η^2 = .500), with slower RTs after valid than invalid cues (450.6 vs 425.7 ms). The latter finding suggests a difficulty to return to cued locations after long cue-target intervals, an effect known as inhibition of return (Posner et al. 1985). Patients with LH-damage had faster RTs to left hemifield targets at the short (609.6 vs 672 ms; $F_{1,11}$ = 13.51, P = .004, η^2 = .551) and long ISI (596.5 vs 670.1 ms; $F_{1,11}$ = 12.62, P = .005, η^2 = .534; Fig. 2b). There was also an effect of validity at the long ISI, with slower RTs following valid than invalid cues (644.2 vs 622.4 ms; $F_{1,11}$ = 5.15, P = .044, η^2 = .319).

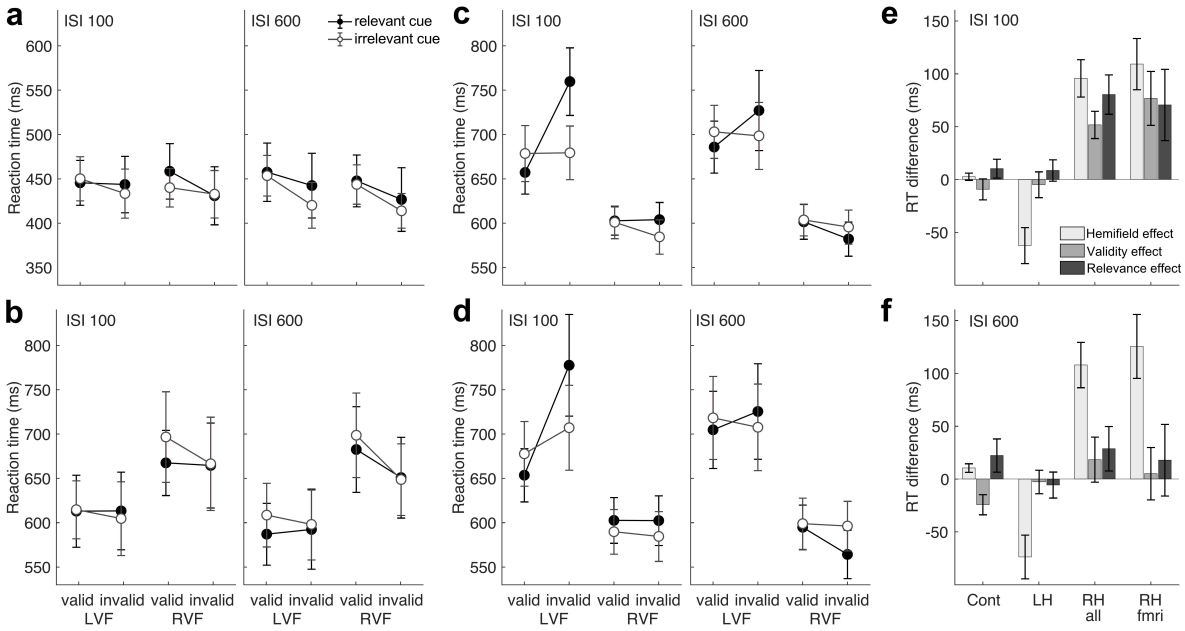

Fig. 2. Behavioral performance. Panels **a-d** show mean reaction times (±SEM) as a function of target position (LVF: left visual field; RVF: right visual field), cue validity and relevance. Each panel shows data for ISI100 on the left and ISI600 on the right. **a**, Healthy controls (Cont; N = 12). **b**, Patients with left hemisphere damage (LH; N = 12). **c**, Patients with right-hemisphere damage (RH all; N = 71). **d**, Sub-set of RH-damaged patients having participated in resting-state fMRI scanning (RH fMRI; N = 26). Note that different scales are used to represent data of healthy controls and the three patient groups. **e**, Bar-plots showing mean (±SEM) hemifield effect, validity effect and relevance effect for all groups (see Methods for the computation of these effects) at ISI100 and **f**, ISI600. Positive values indicate faster RTs to LVF targets than RVF targets (hemifield effect), faster RTs to LVF targets following valid than invalid cues (validity effect) and faster RTs to LVF targets following invalid/irrelevant than invalid/relevant cues (relevance effect).

The RH-group had a different pattern of performance than controls and LH-patients (Fig. 2c), in particular due to strikingly increased RT to left hemifield targets preceded by invalid/relevant cues. At ISI100 these data yielded significant main effects of target position ($F_{1,70}$ = 29.36, P < .001, η^2 = .296), validity ($F_{1,70}$ = 8.64, P = .004, η^2 = .110) and relevance ($F_{1,70}$ = 9.86, P = .002, η^2 = .123), as well as significant two-way interactions of position x

validity ($F_{1,70}$ = 21.05, P < .001, η^2 = .231) and validity x relevance ($F_{1,70}$ = 13.81, P < .001, η^2 = .165). Importantly, a three-way interaction of target position x validity x relevance emerged ($F_{1,70}$ = 13.24, P = .001, η^2 = .159). We performed paired t-tests to examine the source of this interaction, applying Bonferroni-correction to significance levels (α = .0083, two-sided). For targets in the left hemifield we found a highly significant effect of validity for relevant cues (valid/invalid: 657.1 vs 759.6 ms; t_{70} = 4.53, P < .001), but not for irrelevant cues (678.5 vs 679.3 ms; t_{70} = .06, P = .952). Additionally, the comparison of relevant with irrelevant cues in the invalid condition revealed significantly slower RTs for the former than the latter (759.6 vs 679.3 ms; t_{70} = 4.31, P < .001). In the right hemifield we found no effect of validity for relevant cues (valid/invalid: 602.6 vs 603.9 ms; t_{70} = .17, P = .863), but a nearly significant effect for irrelevant cues (t_{70} = 2.44, P = .017). Contrary to the left hemifield this effect was due to slower RTs in the valid condition (600.9 ms) than the invalid condition (584.4 ms). In addition, in the right hemifield invalid cues produced significantly slower RTs when they were relevant (603.9 ms) than when they were irrelevant (584.4 ms; t_{70} = 2.78, P = .007). At ISI600 the pattern of RTs changed notably, as we merely identified a significant effect of target position (left/right hemifield: 703.5 vs 595.6 ms; t_{70} = 25.26, P < .001, η^2 = .265) and a significant trend for the three-way interaction of position x validity x relevance ($F_{1,70}$ = 3.79, P = .056, η^2 = .051).

Thus, RH-damage was associated with a distinctive capture of attention by relevant distracters when cues were shown in the right hemifield and targets in the left hemifield, and this effect was particularly evident at the short ISI. We further examined whether a similar pattern was present in the subgroup of RH patients for whom rs-fMRI scans were available. Fig. 2d shows that the pattern of performance of this subgroup was nearly identical to the entire group of RH-damaged patients. At the short ISI, these data were characterized by significant main effects of target position ($F_{1,25}$ = 20.37, P < .001, η^2 = .449) and validity ($F_{1,25}$ = 6.91, P = .014, η^2 = .216), as well as two-way interactions of position x validity ($F_{1,25}$ = 9.44, P = .005, η^2 = .274) and validity x relevance ($F_{1,25}$ = 7.07, P = .013, η^2 = .220). Critically, the three-way interaction was also significant ($F_{1,25}$ = 6.53, P = .017, η^2 = .207) though none of the post-hoc tests reached significance. At the long ISI there was only a significant effect of target position (left/right hemifield: 720.7 vs. 588.5 ms; $F_{1,25}$ = 17.23, P < .001, η^2 = .408) and an interaction of position x relevance ($F_{1,25}$ = 4.57, P = .043, η^2 = .154).

To compare groups directly, we computed data indexes for the hemifield effect, validity effect and relevance effect (see Methods) and performed a mixed ANOVA with factors group and index type (Fig. 2e and 2f). At the short ISI this analysis revealed only a significant effect of group ($F_{2,92}$ = 7.38, P = .001, η^2 = .138), with higher overall index values in RH-patients (75.9 ms) compared to controls (1.2 ms; t_{81} = 2.38, P = .020) and to LH-patients (-19.5 ms; t_{81} = 3.04, P = .003). The LH-group additionally had lower indexes than controls (t_{22} = 2.46, P = .022). At the long ISI there was only a significant interaction of group x index type ($F_{4,92}$ = 3.14, P = .016, η^2 = .064). Post-hoc tests showed that this interaction was due to larger hemifield effects in RH-patients than LH-patients (107.9 vs -73.7 ms; t_{81} = 3.42, P = .001) and lower hemifield effects in LH-patients than controls (-73.7 vs 10.4 ms; t_{22} = 3.98, P = .001), while the other indices were comparable across groups.

In order to evaluate the impact of handedness, we re-examined the data of all right-handed patients with damage to the right hemisphere (N = 66). This analysis yielded a very similar pattern as the whole RH-group, where the crucial three-way interaction reached significance at the short ISI ($F_{1,65}$ = 10.91, P = .002, η^2 = .144) and was marginal at the long ISI ($F_{1,65}$ = 3.96, P = .051, η^2 = .057). A second potential moderator of the observed interaction between visual field, validity and relevance is spatial neglect. To examine the influence of this factor we performed covariance analyses of the RH-data by adding the number of omissions in the Bells cancellation test and the deviation on the line bisection task as covariates. This analysis revealed for the short ISI a significant interaction between visual field, validity and relevance with the cancellation score ($F_{1,65}$ = 10.94, P = .002, η^2 = .144), but not the bisection score ($F_{1,65}$ = .007, P = .932, η^2 = .0001). At the long ISI, none of the covariates contributed significantly to the three-way interaction.

Together, these results reveal a distinct effect of cue relevance on spatial attention after RH damage when cues are invalid, targets appear contralateral to the lesion and the interval between cue and target is short. Since LH-patients had slower RTs to contralesional targets, yet were not affected by relevance, the impact of relevance appears to be specific to the RH irrespective of general slowing. Contrary to the long-held belief that the main factor affecting attentional disengagement is cue validity (Posner et al. 1984; Losier and Klein 2001) RH-patients only failed to disengage attention when cues share relevant characteristics with the target. In addition, the three-way interaction between visual field, validity and relevance was significantly moderated by the degree of spatial neglect (as measured with a spatial exploration test), indicating that neglect patients exhibit particularly strong capture by highly relevant distracters presented in their intact (right) visual field.

Fig. 3. Lesion overlap plots. Sagittal sections of the Montreal Neurological Institute (MNI) template brain showing color-rendered lesion overlap plots for a, all N = 71 patients with RH-damage, b, subgroup of RH-patients who participated in a fMRI-session (N = 26) and c, N = 12 LH-damaged patients. The color scale indicates the max. number of overlapping lesions and x-values indicate x-location in the MNI-template.

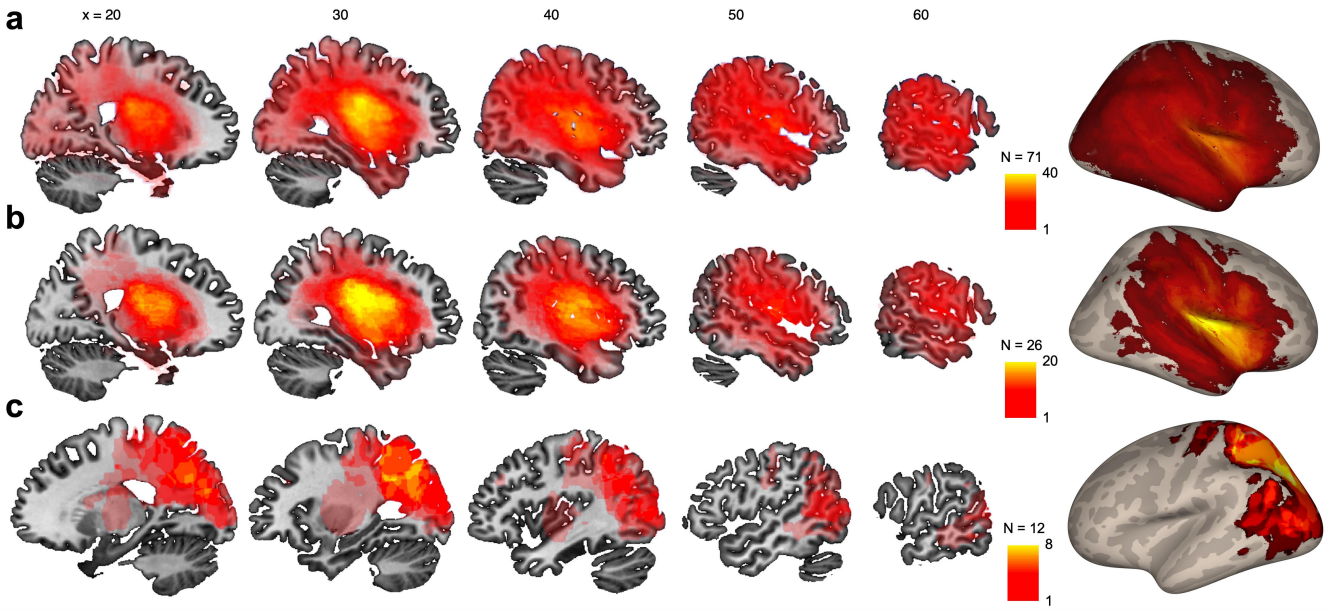

Lesion distributions and lesion-symptom mapping. Fig. 3 shows lesion overlap maps of the RH- and LH-groups and Supplementary Table 1 shows average damage of anatomical structures defined in the Harvard-Oxford atlas. In agreement with previous large-scale studies (Karnath et al. 2004; Pedrazzini and Ptak 2020) lesions in the entire RH-group and the RH-patients involved in the fMRI study tended to cluster subcortically in periventricular white matter. Both groups had damage in the area of the middle cerebral artery, affecting particularly the inferior frontal, the superior temporal and inferior parietal lobe. Importantly, though local damage rarely exceeded 30% of the region volume, all fronto-parietal ROIs were affected in > 12 individual patients. In contrast to the RH-group, LH-patients' lesions were biased toward more posterior sites and mainly affected lateral occipital, inferior and superior parietal cortex.

Since lesion volume is an important unspecific predictor of behavioral symptoms (Mah et al. 2014; DeMarco and Turkeltaub 2018), we first examined the relationship between damage at each specific voxel and lesion volume. We computed a z-score for individual volumes by thresholding them to all 71 lesion volumes and then averaged the obtained z-scores across all lesions at each damaged voxel. The resulting volume bias plot (Supplementary Fig. 1a) shows voxel-wise probability that damage is associated with lesion volume. Out of nine regions of interest (ROIs) covering the area of the right middle cerebral artery, the largest lesion volume was associated with damage to the superior parietal lobule (SPL), while insula and mid-PFC (mPFC) were linked to comparatively small lesions (Supplementary Fig. 1b). This finding indicates that large lesions are necessary for damage to occur in the SPL, while the likelihood of being damaged even with small lesions is much greater for the insular cortex. This effect of lesion volume presents a potential bias in lesion-behavior relationships, and our data therefore underscore the necessity to control for regional volume bias.

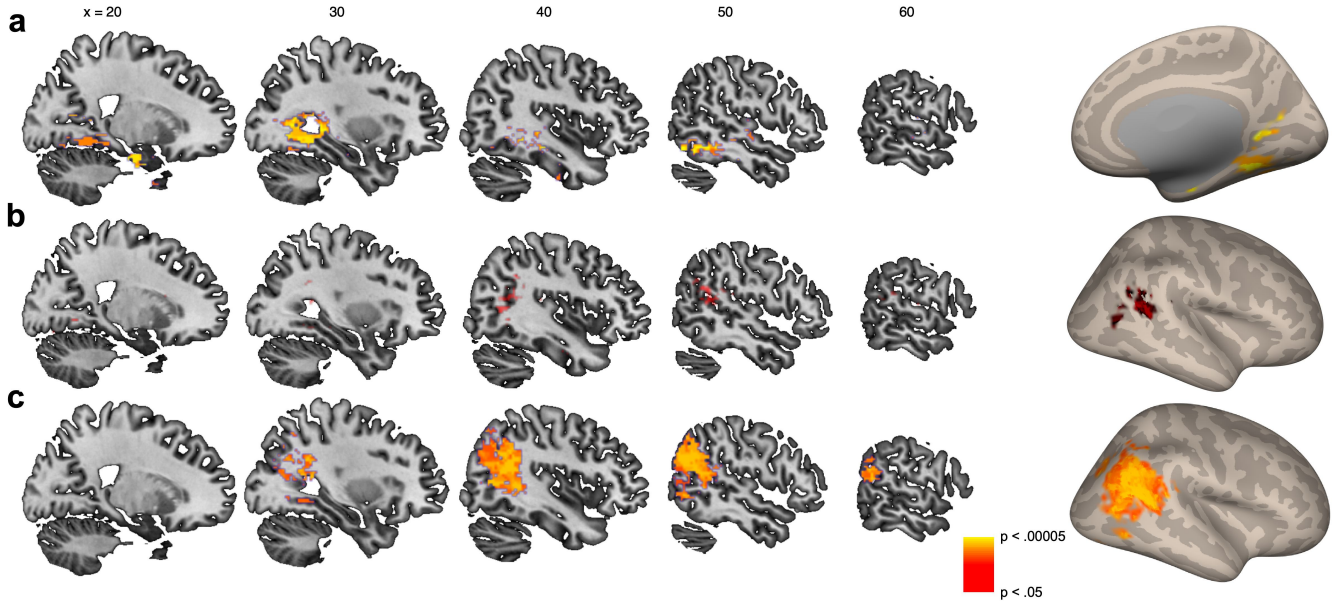

Fig. 4. Results of SVR-LSM. a, Sagittal sections of the Montreal Neurological Institute (MNI) template brain showing the brain region identified as significant predictor of the hemifield effect. **b**, Brain region whose damage is associated with an increased validity effect (note that the voxels presented here reached voxel-level significance p < 0.005, but not permutation-derived cluster-level significance). **c**, Brain region identified as significant predictor of the relevance effect. The right side shows cortical projections of these brain areas on an inflated brain. Scale shows permutation-derived cluster-level significance and x-values indicate x-location in the MNI-template.

Next, we performed lesion-symptom mapping (LSM) using support vector regression (SVR). The aim of these analyses was to identify in the lesion data of all 71 RH-damaged patients the possible anatomical predictors of the hemifield effect, validity effect and relevance effect. All analyses were performed on 54016 voxels damaged in at least five patients, by including lesion volume as nuisance variable in lesion data and behavioral scores. SVR-LSM of the hemifield effect identified one significant cluster (Fig. 4a; N = 1601 voxels) in the right fusiform and lingual gyrus, extending into the ventral lateral occipital cortex (LOC). Analysis of the validity effect did not detect any voxels reaching cluster-level statistical threshold. The closest to statistical significance (P = .114) was a cluster of 403 voxels lying at the right TPJ (Fig. 4b). In contrast, we identified a large cluster of 3498 voxels whose damage was significantly associated with an increased relevance effect (Fig. 4c). The cluster was located at the right TPJ, overlapping with dorsal LOC (dLOC), inferior angular gyrus and posterior part of the superior temporal gyrus (STG). In order to exclude a contribution of visual field deficits we repeated these analyses, but added visual field impairment as nuisance factor. This nullified the previously identified cluster of voxels associated with the hemifield effect, but had only a negligible effect on the cluster predicting the relevance effect, which barely shrank to N = 3472 voxels. To further control for the impact of spatial neglect we computed a neglect index by averaging the number of left-sided relative to right-sided omissions in two cancellation tests (Methods) and re-analyzed the relevance index with visual field and neglect index as covariates. Even after including these two nuisance variables, the area (N = 3690 voxels) overlapping the right TPJ and dLOC remained a significant predictor of the relevance effect.

Given that we found no significant anatomical predictor of the validity effect we conducted additional SVR-LSMs separately for relevant and irrelevant cues. Analysis of the validity effect with relevant cues again identified a significant cluster at the right TPJ (N = 1124 voxels), located at the intersection between the inferior angular gyrus and posterior STG (Supplementary Fig. 2a). In contrast, the validity effect with irrelevant cues was not associated with any significant anatomical predictors. Closest to significance (P = .067) was a cluster of 711 voxels located in white matter of the centrum semiovale (Supplementary Fig. 2b).

Thus, a region including the right TPJ and extending into the dLOC was a strong predictor of the relevance effect, irrespective of the presence of visual field impairment or degree of spatial neglect. In addition, this region was not associated with attentional disengagement in general, but specifically with reorienting following relevant cues.

Resting-state functional connectivity. In order to obtain a global picture of rs-fMRI connectivity patterns, we first examined FC within and between the hemispheres, by taking into account all ROIs. Supplementary Fig. 3a displays ROI-to-ROI connectivity matrices and Supplementary Fig. 3b shows the same data in a bee-swarm plot,

separately for intrahemispheric and interhemispheric ROI-pairs. In agreement with the more elongated shape of these plots, F-tests revealed higher dispersion of the control data (all P < .001), except for interhemispheric homotopic FC (P = .967). T-tests comparing mean FC showed that RH-intrahemispheric connectivity (controls: 0.046; patients: 0.042, t_{2448} = .29, P = .78) and heterotopic interhemispheric connectivity (controls: 0.017; patients: 0.010; t_{2448} = 0.62, P = .537) were indistinguishable between groups. In contrast, LH-connectivity was slightly, yet significantly higher in patients (0.028 vs 0.055; t_{2448} = 1.98, P = .048), while homotopic FC was significantly higher in controls (0.723 vs 0.098; t_{98} = 6.29, P < .001). Patients thus showed a compensatory increase of FC within their intact LH, but strongly decreased interhemispheric connectivity between homotopic regions. We inspected FC in more detail for nine homotopic ROIs of the dorsal and ventral attention network (see Methods). Healthy controls exhibited higher FC for all ROIs (all t_{51} > 3.2, P < .002) except the IC and dPFC. We also checked whether homotopic FC between either of these ROIs correlated with the hemifield effect, validity effect or relevance effect; however, none of these correlations reached significance.

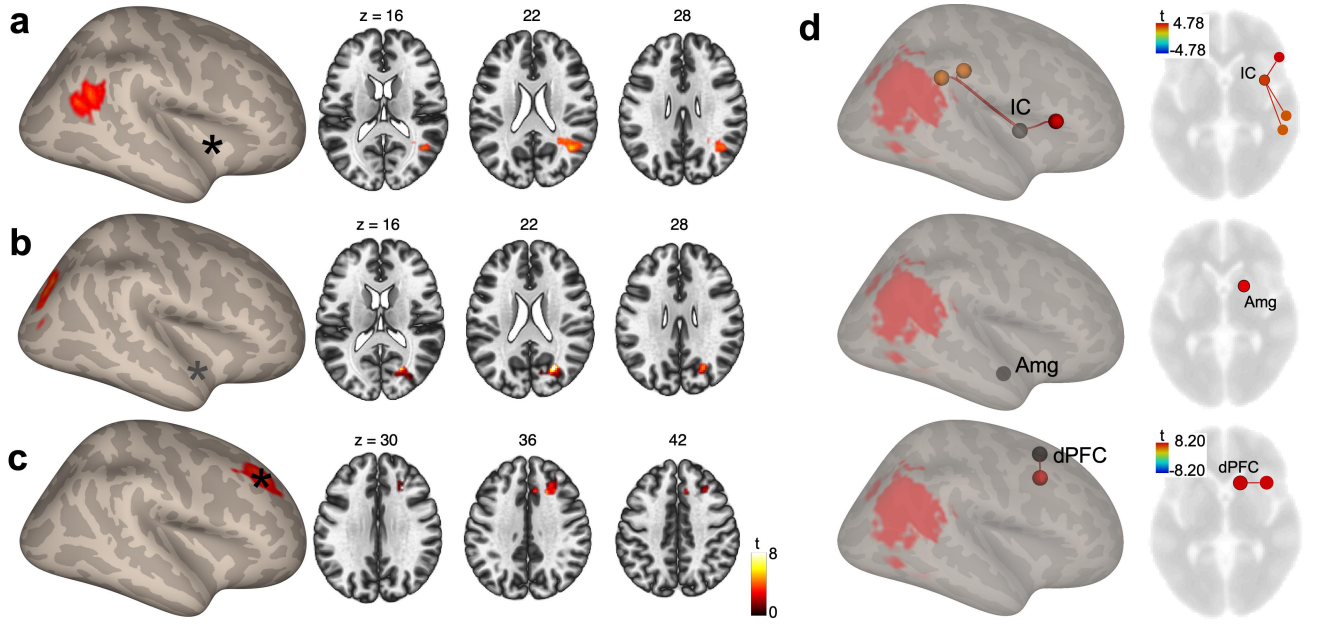

Fig. 5. Seed-based and ROI-based connectivity in patients. a, Seed-to-voxel connectivity between right IC and angular gyrus/dLOC predicting an increased relevance effect in patients with RH damage. **b**, FC between the right amygdala and posterior intraparietal sulcus/dLOC is also significantly associated with the relevance effect. **c**, In contrast, the relevance effect is only associated with local connectivity between the dPFC and mPFC, but no antero-posterior connectivity. **d**, ROI-to-ROI connectivity of IC (top), amygdala (Amg; middle) and dPFC (bottom) projected on an inflated brain. The right side shows the same connections, shown on axial sections of the template brain. The red overlay shows the region of damage associated with the relevance effect in the SVR-LSM analysis, and the star shows the center of each seed-ROI and z-values indicate z-location in the MNI-template.

We next examined FC predictors of behavioral performance by systematically testing seed-to-voxel connectivity, where each right-hemispheric ROI was successively defined as seed, any other voxel of the brain was a potential target, and the respective contribution of the hemifield, validity and relevance effect was partialled out. None of these analyses yielded a significant finding for the hemifield effect and the validity effect, but three predictors were identified for the relevance effect. The first was FC between the insular cortex (IC) and the right inferior angular gyrus, posterior superior temporal sulcus and dLOC (cluster-x,y,z: 40,-58,22; 198 voxels; P = .015; Fig. 5a). This region corresponds to the center of the rTPJ area identified as significant predictor of the relevance effect in the SVR-LSM analyses. The second predictor was connectivity between the amygdala, the ascending branch of the right intraparietal sulcus and the dLOC (x,y,z: 22,-70,20; 158 voxels; P = .016; Fig. 5b). The third source of significant FC was the dPFC (x,y,z: 26, 32, 36; 233 voxels; P = .003; Fig. 4c), which however only connected with closely neighboring regions including mPFC.

These analyses demonstrate that functional interactions between two regions of the saliency network (IC and amygdala) and the inferior parietal/superior occipital cortex predict increased attentional capture by relevant cues. To characterize further these patterns of FC, we examined ROI-to-ROI interactions between IC, amygdala, dPFC, and five other ROIs known to constitute the attention network (see Methods). These analyses were based on average FC computed within each ROI. As shown in Fig. 4d the IC was significantly connected with ventral PFC (vPFC), the supramarginal gyrus (SMG) and angular gyrus, whereas amygdala connectivity did not reach significance, and the dPFC only connected with mPFC. In agreement with the voxel-wise analyses, ROI-to-ROI statistics thus confirmed significant insulo-parietal FC and only local connectivity of the dPFC.

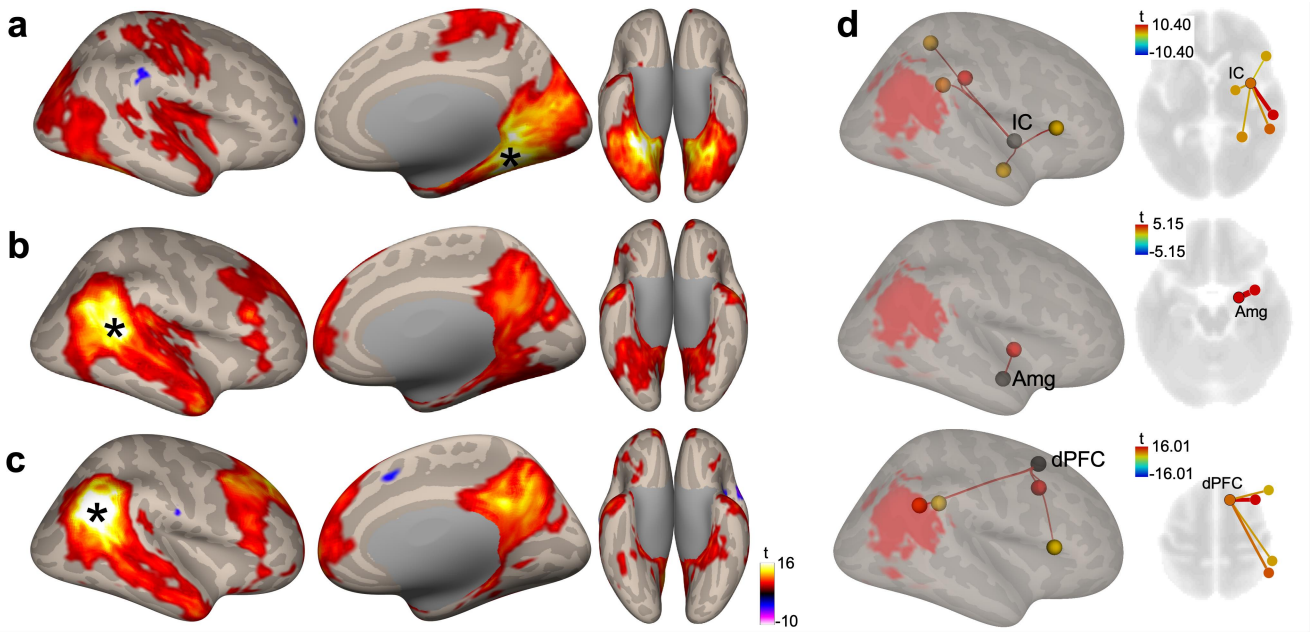

Fig. 6. Seed-based and ROI-based connectivity in healthy controls. a, Seed-to-voxel FC between the brain region that was a predictor of the hemifield effect in SVR-LSM analyses and the rest of the brain. Though the seed is in the inferior temporal and vLOC, significant connectivity with the posterior insula and dorsal fronto-parietal regions is identified. **b** and **c**, FC between anatomical predictors of the validity (**b**) and relevance effect (**c**). **d**, ROI-to-ROI connectivity of IC (top), amygdala (Amg; middle) and dPFC (bottom) projected on an inflated brain. The right side shows the same connections, shown on axial sections of the template brain. The red overlay shows the region of damage associated with the relevance effect in the SVR-LSM analysis, and the star shows the center of each seed-ROI and z-values indicate z-location in the MNI-template.

In order to examine whether these findings reflect a pattern of functional connection/disconnection specific to patients we next analyzed seed-based and ROI-based FC in a sample of healthy participants. In a first step we defined each of the three brain regions identified in the lesion analyses (see Fig. 3) as seed for a seed-to-voxel analysis. This analysis revealed that the right infero-temporal area predicting the hemifield effect was functionally connected with large areas of lateral occipital, inferior temporal, insular and fronto-parietal cortex (Fig. 6a). Seeds derived from lesion analyses of validity and relevance effects yielded similar FC patterns, which is not surprising given their anatomical overlap. Both were functionally connected to the middle and superior temporal gyrus, the retro-splenial cortex, the frontal pole and the dPFC (Fig. 6b, c). We finally performed ROI-to-ROI analyses, focusing on the connections between the IC, amygdala or dPFC with other regions of the right attention network (Fig. 6d). These analyses revealed significant connectivity between IC and SMG, superior parietal cortex, vPFC and amygdala. The latter structure was only connected to the IC, while the dPFC had significant FC with the SMG, angular gyrus, mPFC and vPFC. In sum, the IC and dPFC were each functionally connected with ROIs lying at the TPJ, and thus within the area whose damage was a significant predictor of increased relevance effects in patients. These data contrast with those of patients, who only showed significant FC between the insula and rTPJ, while the dPFC appeared to be functionally isolated.

Discussion

Our results demonstrate that functional interactions between the right TPJ, insula and dPFC play a decisive role for the control of spatial attention when behaviorally relevant distracters are present. Two new conclusions emerge from our findings: first, we show that damage to the right TPJ only results in exaggerated capture of attention by distracters if these are behaviorally relevant. This finding contradicts previous studies postulating a generalized deficit of attentional disengagement after rTPJ damage, irrespective of specific cue characteristics or similarities between cue and target. Second, analyses of resting-FC indicate that the distracting effect of relevant stimuli depends on functional interactions between core regions of the saliency network and the rTPJ.

The rTPJ is biased toward relevance. Our findings are consistent with previous lesion studies showing that damage to the rTPJ leads to pathological capture of attention, together with the failure to disengage attention from stimuli appearing in the right hemifield (Posner et al. 1984; Friedrich et al. 1998). LH- and RH-patient groups

showed significant slowing of RTs to targets appearing in the hemifield opposite their lesion, but only the RH-group also exhibited increased validity and relevance effects. This specificity of RH-damage shows that contralesional slowing is not a sufficient condition for the occurrence of validity and relevance effects. Though the LH-group was too small to allow conclusive judgment, our findings agree with previous studies regarding the dominance of the RH for the shifting and disengagement of attention. Unfortunately, most previous studies did not provide detailed anatomical information and involved much smaller numbers of participants (Bartolomeo et al. 2001; Ptak and Schnider 2006; Bonato et al. 2009), which makes it difficult to attribute pathological capture of attention to the presence of spatial neglect, damage to a specific brain area, or a combination of both factors. Our SVR-LSM analyses clarify this issue by showing that rTPJ damage is crucial for the occurrence of pathological capture, even if visual field impairment and degree of neglect are controlled for. The machine learning approach applied here also effectively controls for the influence of lesion volume and anatomical bias attributable to brain vascularization, two powerful confounds in lesion-mapping studies (DeMarco and Turkeltaub 2018).

A centerpiece of the behavioral results is the observation that pathological capture of attention after rTPJ damage is contingent on the behavioral relevance of the cue. A prominent cognitive model defends the viewpoint that engagement of attention is either voluntary or reflexive, but in any case, is essentially determined by the spatial disposition and physical saliency of stimuli (Posner and Petersen 1990; Petersen and Posner 2012). Consequently, previous studies of spatial attention in patients with RH-damage used a single type of cue and focused on the validity effect rather than interactions between target position and cue relevance (Posner et al. 1984; Bartolomeo et al. 2001; Losier and Klein 2001; Corbetta et al. 2005). These findings have been taken as evidence that patients with spatial neglect after RH-damage show general failure to reorient attention following a right-lateralized cue, in particular if stimulus-driven processes are involved (Losier and Klein 2001; Bartolomeo and Chokron 2002). Our results show that controlling for cue relevance is pivotal, as the validity effect is manifestly driven by the behavioral relevance of cues, and entirely disappears when cues are irrelevant. This critical role of cue relevance is also confirmed by the SVR-LSM analyses. While validity effects of relevant cues were associated with significant damage to the rTPJ, no definite anatomical substrate emerged with irrelevant cues.

Together, these findings challenge the proposal that the rTPJ redirects attention toward any salient, infrequent or unexpected event, irrespective of its connection to the target (Corbetta et al. 2008). The main effect of rTPJ damage appears to be an increased sensibility to task-relevant information, while the shifting of attention following the presentation of irrelevant information is unaffected. Additionally, our rs-fMRI findings indicate that the primary role of the rTPJ must be evaluated in the context of functional interactions of this region with other brain regions.

Functional connectivity predicts capture of attention. In agreement with previous findings (He et al. 2007; Carter et al. 2010; Siegel et al. 2016; Ptak et al. 2020), RH-patients exhibited widespread changes of FC, in particular a decrease of homotopic, cross-hemispheric connectivity. By contrast, while previous reports found that interhemispheric FC correlates with the degree of spatial deficit (He et al. 2007; Carter et al. 2010; Ptak et al. 2020), we only identified significant predictors of behavior in RH intrahemispheric FC. As our results suggest, even within the same visuo-spatial task different indices of performance may dissociate across the hemispheres, as the hemifield effect (which was similarly affected by unilateral LH or RH damage) and the validity/relevance effects (which were only impacted in patients with RH lesions) did in our samples. Interhemispheric FC-behavior relationships may therefore depend on the amount of residual connectivity between the hemispheres, as well as on the importance of collaboration between the two hemispheres during different cognitive tasks.

Seed-based FC revealed a connection between the right IC and right TPJ that predicted the relevance effect. This finding is complemented by a significant connection between the amygdala and right dLOC, a region lying close to the area of damage predicting the relevance effect. These two core components of the saliency network are important for motivational aspects of behavior, in particular regarding salient external or interoceptive signals. Current models attribute to the IC the role of a ‘switch’ that may detect and signal incongruent stimuli requiring an interruption of current activity and the mobilization of cognitive resources for an adequate response (Jones et al. 2010; Menon and Uddin 2010; Chang et al. 2013). Stimuli activating the IC often entail a prioritized response, as they may signal immediate threats (e.g., pain), aversive experiences (e.g., disgust), or even isolated ‘oddball’ items (Uddin 2015). However, this proposal does not explain how the IC integrates with attention networks in the presence of highly relevant information. Our results show that a functional connection between the saliency network and the right posterior cortex exists, and that this connection predicts the modulation of attention by spatial cues with target-defining features.

Recent parcellation work with healthy participants has suggested two (Shirer et al. 2012) or three (Chang et al. 2013) functional subdivisions of the insular cortex: a ventroanterior portion connected to limbic areas including the amygdala and orbitofrontal cortex, a dorsoanterior portion connected with the anterior cingulate cortex and dPFC, and a posterior portion connected to premotor and somatosensory cortex. The dorsoanterior insula also has network connections with ventral premotor cortex and the rTPJ (Touroutoglou et al. 2012). While our findings do not allow identifying the precise area in the insula that maintains a functional connection with the rTPJ (the insula

ROI defined with the Harvard-Oxford atlas covers the entire insular cortex), they complement these parcellation studies in suggesting a functional role of (parts of) the IC in the orienting of attention.

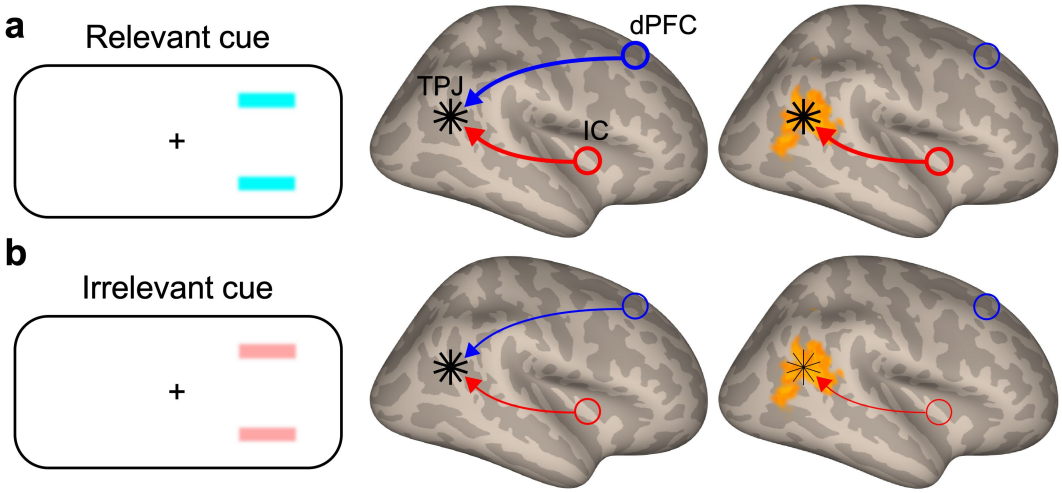

Fig. 7. Interactive model of attention capture. a, Processing of relevant distracters in the healthy brain (middle panel) and after rTPJ damage (right panel). The right IC is automatically activated by task-relevant features and strongly activates the rTPJ (red arrow). In the healthy brain the dPFC regulates the extent of activation at the rTPJ (blue arrow). This top-down regulation is lacking in patients with rTPJ damage, resulting in a bias of attention toward task-relevant information. **b**, Processing of irrelevant distracters in healthy subjects (middle) and after rTPJ damage (right). Activation of the rTPJ by the IC and its modulation by the dPFC cancel each other in healthy subjects, the net result being that the rTPJ is similarly activated by relevant and irrelevant distracters. After rTPJ damage, the weak rTPJ activation by the IC is insufficient to produce significant capture of attention by irrelevant stimuli. The star-shape at the TPJ indicates the degree of activation.

An interactive model of spatial attention. The functional connection between the saliency network and the rTPJ explains the prioritization of relevant cues, yet the size of the effect remains puzzling. Why were patients unable to resist the distracting effect of these cues? Relevant cues only captured attention at the short ISI, suggesting a reflexive and short-lived effect. Previous lesion studies argued that interactions between the dPFC and posterior parietal cortex or the TPJ are important for the control of spatial attention (Barcelo et al. 2000; Ptak and Schnider 2010; Fellrath et al. 2016). Remarkably, while our healthy participants exhibited significant seed-based and ROI-based dPFC - rTPJ connectivity, the dPFC of patients appeared to be functionally isolated. Since the dPFC was relatively preserved, this finding suggests a true functional disconnection, not the effect of damage to this region.

Together, our findings support an interactive model of the modulation and control of attention where the IC and dPFC have complementary effects on the rTPJ (Fig. 7). We propose that the saliency network biases the ventral attention network in a tonic way towards stimuli of high motivational value. In the healthy brain, behaviorally relevant distracters will have the tendency to interrupt current activity by activating the rTPJ, but this activity is in turn modulated by top-down signals from the dPFC. Our findings suggest that following damage to the rTPJ, the IC continues to bias TPJ activity, while the modulating influence from the dPFC is absent. As a consequence, task activity is easily interrupted, and attention is strongly biased towards behaviorally relevant events, while disengagement of attention from irrelevant stimuli is unaffected.

Caveats and conclusions. The involvement of brain-injured participants necessarily adds some limitations to the present study. First, in order to obtain a large sample, we included patients irrespective of handedness. Though our analyses did not identify significant handedness effects, such effects might become visible in larger samples. In addition, because of their hemiplegia several LH-damaged patients were forced to respond with their non-dominant hand, which might have affected their RT patterns. A second point concerns the definition of ROIs used in the connectivity study. Our analyses were not based on a-priori hypotheses concerning the insula or any other brain region; for this reason, we applied a brain atlas in which ROIs are defined based on structural characteristics. However, an increasing number of studies have identified functional units of the insula, whereby anterior and posterior sub-divisions connect with distinct brain regions and are involved in different cognitive, affective and bodily functions (Shirer et al. 2012; Chang et al. 2013). Similarly, the TPJ is not a functionally homogenous brain region, but has been implicated in diverse functions, such as attention, memory or social cognition (Decety and Lamm 2007; Mars et al. 2012; Carter and Huettel 2013). It is therefore possible that future

studies provide a more fine-grained analysis of insular and TPJ regions crucial for the modulation of attention by stimulus relevance. Finally, an interesting topic is whether our mechanistic account of insula, TPJ and dPFC interactions can be extended to include the contribution of posterior parietal cortex, a region that plays a crucial role in the construction of spatial priority maps (Vandenberghe et al. 2012; Ptak and Fellrath 2013; Chelazzi et al. 2014). Even though the present results do not inform us about the role of this region, we believe that the study of functional interactions between damaged and intact brain regions will play an essential role for the understanding of attention networks in the human brain.

References

Anderson BA, Laurent PA, Yantis S. 2011. Value-driven attentional capture. Proc Natl Acad Sci U S A. 108:10367-10371.

Awh E, Belopolsky AV, Theeuwes J. 2012. Top-down versus bottom-up attentional control: a failed theoretical dichotomy. Trends Cogn Sci. 16:437-443.

Baluch F, Itti L. 2011. Mechanisms of top-down attention. Trends in Neurosciences. 34:210-224.

Barcelo F, Suwazono S, Knight RT. 2000. Prefrontal modulation of visual processing in humans. Nature Neurosci. 3:399-403.

Bartolomeo P, Chokron S. 2002. Orienting of attention in left unilateral neglect. Neurosci Biobehav Rev. 26:217-234.

Bartolomeo P, Siéroff E, Decaix C, Chokron S. 2001. Modulating the attentional bias in unilateral neglect: the effects of the strategic set. Exp Brain Res. 137:432-444.

Bonato M, Priftis K, Marenzi R, Zorzi M. 2009. Normal and impaired reflexive orienting of attention after central nonpredictive cues. J Cogn Neurosci. 21:745-759.

Caballero-Gaudes C, Reynolds RC. 2017. Methods for cleaning the BOLD fMRI signal. NeuroImage. 154:128-149.

Carter AR, Astafiev SV, Lang CE, Connor LT, Rengachary J, Strube MJ, Pope DL, Shulman GL, Corbetta M. 2010. Resting interhemispheric functional magnetic resonance imaging connectivity predicts performance after stroke. Ann Neurol. 67:365-375.

Carter RM, Huettel SA. 2013. A nexus model of the temporal-parietal junction. Trends Cogn Sci. 17:328-336.

Cave KR, Bichot NP. 1999. Visuospatial attention: beyond a spotlight model. Psychonom Bull Rev. 6:204-223.

Chang LJ, Yarkoni T, Khaw MW, Sanfey AG. 2013. Decoding the role of the insula in human cognition: functional parcellation and large-scale reverse inference. Cereb Cortex. 23:739-749.

Chelazzi L, Estocinova J, Calletti R, Lo Gerfo E, Sani I, Della Libera C, Santandrea E. 2014. Altering spatial priority maps via reward-based learning. J Neurosci. 34:8594-8604.

Corbetta M, Kincade MJ, Lewis C, Snyder AZ, Sapir A. 2005. Neural basis and recovery of spatial attention deficits in spatial neglect. Nature Neurosci. 8:1603-1610.

Corbetta M, Patel G, Shulman GL. 2008. The reorienting system of the human brain: from environment to theory of mind. Neuron. 58:306-324.

Corbetta M, Shulman GL. 2002. Control of goal-directed and stimulus-driven attention in the brain. Nat Rev Neurosci. 3:201-215.

Coull JT, Nobre AC. 1998. Where and when to pay attention: The neural systems for directing attention to spatial locations and to time intervals as revealed by both PET and fMRI. J Neurosci. 18:7426-7435.

Decety J, Lamm C. 2007. The role of the right temporoparietal junction in social interaction: how low-level computational processes contribute to meta-cognition. Neuroscientist. 13:580-593.

DeMarco AT, Turkeltaub PE. 2018. A multivariate symptom mapping toolbox and examination of lesion-volume biases and correction methods in lesion-symptom mapping. Human Brain Mapping. 39:4169-4182.

Desikan RS, Segonne F, Fischl B, Quinn BT, Dickerson BC, Blacker D, Buckner RL, Dale AM, Maguire RP, Hyman BT, Albert MS, Killiany RJ. 2006. An automated labeling system for subdividing the human cerebral cortex on MRI scans into gyral based regions of interest. NeuroImage. 31:968-980.

Egeth HW, Yantis S. 1997. Visual attention: control, representation, and time course. Ann Rev Psychol. 48:269-297.

Eimer M, Kiss M. 2008. Involuntary attentional capture is determined by task set: evidence from event-related brain potentials. J Cogn Neurosci. 20:1423-1433.

Fellrath J, Mottaz A, Schnider A, Guggisberg AG, Ptak R. 2016. Theta-band functional connectivity in the dorsal fronto-parietal network predicts goal-directed attention. Neuropsychologia. 92:20-30.

Folk CL, Remington RW, Johnston JC. 1992. Involuntary covert orienting is contingent on attentional control settings. J Exp Psychol: Hum Percept Perf. 18:1030-1044.

Friedrich FJ, Egly R, Rafal RD, Beck D. 1998. Spatial attention deficits in humans: A comparison of superior parietal and temporal-parietal junction lesions. Neuropsychology. 12:193-207.

Gauthier L, Dehaut F, Joanette Y. 1989. The Bells Test: A quantative and qualitative test for visual neglect. Int J Clin Neuropsychol. 11:49-54.

Ghaleh M, Lacey EH, Fama ME, Anbari Z, DeMarco AT, Turkeltaub PE. 2020. Dissociable mechanisms of working memory revealed through multivariate lesion mapping. Cereb Cortex. 30:2542-2554.

Gilbert CD, Li W. 2013. Top-down influences on visual processing. Nat Rev Neurosci. 14:350-363.

Goveas JS, Xie C, Chen G, Li W, Ward BD, Franczak MB, Jones JL, Antuono PG, Li SJ. 2013. Functional network endophenotypes unravel the effects of apolipoprotein E epsilon 4 in middle-aged adults. PLoS One. 8:e55902.

He BJ, Snyder AZ, Vincent JL, Epstein A, Shulman GL, Corbetta M. 2007. Breakdown of functional connectivity in frontoparietal networks underlies behavioral deficits in spatial neglect. Neuron. 53:905-918.

Indovina I, Macaluso E. 2007. Dissociation of stimulus relevance and saliency factors during shifts of visuospatial attention. Cereb Cortex. 17:1701-1711.

Itti L, Koch C. 2001. Computational modelling of visual attention. Nat Rev Neurosci. 2:194-203.

Jones CL, Ward J, Critchley HD. 2010. The neuropsychological impact of insular cortex lesions. J Neurol Neurosurg Psychiatry. 81:611-618.

Karnath HO, Fruhmann Berger M, Küker W, Rorden C. 2004. The anatomy of spatial neglect based on voxelwise statistical analysis: A study of 140 patients. Cereb Cortex. 14:1164-1172.

Kincade JM, Abrams RA, Astafiev SV, Shulman GL, Corbetta M. 2005. An event-related functional magnetic resonance imaging study of voluntary and stimulus-driven orienting of attention. J Neurosci. 25:4593-4604.

Knudsen EI. 2007. Fundamental components of attention. Ann Rev Neurosci. 30:57-78.

Losier BJW, Klein RM. 2001. A review of the evidence for a disengage deficit following parietal lobe damage. Neurosci Biobehav Rev. 25:1-13.

Mah Y-H, Husain M, Rees G, Nachev P. 2014. Human brain lesion-deficit inference remapped. Brain. 137:2522-2531.

Maljkovic V, Nakayama K. 1994. Priming of pop-out: I. Role of features. Mem Cog. 22:657-672.

Mars RB, Sallet J, Schüffelgen U, Jbabdi S, Toni I, Rushworth MFS. 2012. Connectivity-based subdivisions of the human right "temporoparietal junction area": Evidence for different areas participating in different cortical networks. Cereb Cortex. 22:1894-1903.

Menon V, Uddin LQ. 2010. Saliency, switching, attention and control: a network model of insula function. Brain Struct Funct. 214:655-667.

Nachev P, Coulthard E, Jager HR, Kennard C, Husain M. 2008. Enantiomorphic normalization of focally lesioned brains. NeuroImage. 39:1215-1226.

Pedrazzini E, Ptak R. 2019. Damage to the right temporoparietal junction, but not lateral prefrontal or insular cortex, amplifies the role of goal-directed attention. Scientific Reports. 9:306.

Pedrazzini E, Ptak R. 2020. The neuroanatomy of spatial awareness: a large-scale region-of-interest and voxel-based anatomical study. Brain Imaging and Behavior. 14:615-626.

Petersen SE, Posner MI. 2012. The attention system of the human brain: 20 years after. Ann Rev Neurosci. 35:73-89.

Posner MI, Petersen SE. 1990. The attention system of the human brain. Ann Rev Neurosci. 13:25-42.

Posner MI, Rafal RD, Choate LS, Vaughan J. 1985. Inhibition of return: Neural basis and function. Cogn Neuropsychol. 2:211-228.

Posner MI, Walker JA, Friedrich FJ, Rafal RD. 1984. Effects of parietal injury on covert orienting of attention. J Neurosci. 4:1863-1874.

Power JD, Barnes KA, Snyder AZ, Schlaggar BL, Petersen SE. 2012. Spurious but systematic correlations in functional connectivity MRI networks arise from subject motion. NeuroImage. 59:2142-2154.

Ptak R. 2012. The frontoparietal attention network of the human brain: Action, saliency, and a priority map of the environment. Neuroscientist. 18:502-515.

Ptak R, Bourgeois A, Cavelti S, Doganci N, Schnider A, Iannotti GR. 2020. Discrete patterns of cross-hemispheric functional connectivity underlie impairments of spatial cognition after stroke. J Neurosci. 40:6638-6648.

Ptak R, Di Pietro M, Schnider A. 2012. The neural correlates of object-centered processing in reading: A lesion study of neglect dyslexia. Neuropsychologia. 50:1142-1150.

Ptak R, Fellrath J. 2013. Spatial neglect and the neural coding of attentional priority. Neurosci Biobehav Rev. 37:705-722.

Ptak R, Schnider A. 2006. Reflexive orienting in spatial neglect is biased towards behaviourally salient stimuli. Cereb Cortex. 16:337-345.

Ptak R, Schnider A. 2010. The dorsal attention network mediates orienting toward behaviorally relevant stimuli in spatial neglect. J Neurosci. 30:12557-12565.

Ptak R, Schnider A, Golay L, Müri R. 2007. A non-spatial bias favouring fixated stimuli revealed in patients with spatial neglect. Brain. 130:3211-3222.

Ronchi R, Algeri L, Chiapella L, Spada S, Vallar G. 2012. Spatial neglect and perseveration in visuomotor exploration. Neuropsychology. 26:588-603.

Rorden C, Bonilha L, Fridriksson J, Bender B, Karnath HO. 2012. Age-specific CT and MRI templates for spatial normalization. NeuroImage. 61:957-965.

Rorden C, Karnath H-O, Bonilha L. 2007. Improving lesion-symptom mapping. J Cogn Neurosci. 19:1081-1088.

Royall DR, Cordes JA, Polk M. 1998. CLOX: an executive clock drawing task. J Neurol Neurosurg Psychiatry. 64:588-594.

Seeley WW, Menon V, Schatzberg AF, Keller J, Glover GH, Kenna H, Reiss AL, Greicius MD. 2007. Dissociable intrinsic connectivity networks for salience processing and executive control. J Neurosci. 27:2349-2356.

Serences JT, Shomstein S, Leber AB, Golay X, Egeth HE, Yantis S. 2005. Coordination of voluntary and stimulus-driven attentional control in human cortex. Psychol Sci. 16:114-122.

Shirer WR, Ryali S, Rykhlevskaia E, Menon V, Greicius MD. 2012. Decoding subject-driven cognitive states with whole-brain connectivity patterns. Cereb Cortex. 22:158-165.

Shulman GL, Astafiev SV, Franke D, Pope DL, Snyder AZ, McAvoy MP, Corbetta M. 2009. Interaction of stimulus-driven reorienting and expectation in ventral and dorsal frontoparietal and basal ganglia-cortical networks. J Neurosci. 29:4392-4407.

Siegel JS, Ramsey LE, Snyder AZ, Metcalf NV, Chacko RV, Weinberger K, Baldassarre A, Hacker CD, Shulman GL, Corbetta M. 2016. Disruptions of network connectivity predict impairment in multiple behavioral domains after stroke. Proc Natl Acad Sci U S A. 113:E4367-4376.

Simons DJ. 2000. Attentional capture and inattentional blindness. Trends Cogn Sci. 4:147-155.

Sperber C, Karnath HO. 2017. Impact of correction factors in human brain lesion-behavior inference. Hum Brain Mapp. 38:1692-1701.

Sperber C, Karnath HO. 2018. On the validity of lesion-behaviour mapping methods. Neuropsychologia. 115:17-24.

Sperber C, Wiesen D, Karnath HO. 2019. An empirical evaluation of multivariate lesion behaviour mapping using support vector regression. Hum Brain Mapp. 40:1381-1390.

Szczepanski SM, Konen CS, Kastner S. 2010. Mechanisms of spatial attention control in frontal and parietal cortex. J Neurosci. 30:148-160.

Theeuwes J. 2010. Top-down and bottom-up control of visual selection. Acta Psychol. 135:77-99.

Touroutoglou A, Hollenbeck M, Dickerson BC, Feldman Barrett L. 2012. Dissociable large-scale networks anchored in the right anterior insula subserve affective experience and attention. NeuroImage. 60:1947-1958.

Uddin LQ. 2015. Salience processing and insular cortical function and dysfunction. Nat Rev Neurosci. 16:55-61.

Vandenberghe R, Molenbergs P, Gillebert CR. 2012. Spatial attention deficits in humans: the critical role of superior compared to inferior parietal lesions. Neuropsychologia. 50:1092-1103.

Whitfield-Gabrieli S, Nieto-Castanon A. 2012. Conn: a functional connectivity toolbox for correlated and anticorrelated brain networks. Brain Connectivity. 2:125-141.

Zhang Y, Kimberg DY, Coslett HB, Schwartz MF, Wang Z. 2014. Multivariate lesion-symptom mapping using support vector regression. Human Brain Mapping. 35:5861-5876.

Supplementary Information for

Insular cortex mediates attentional capture by behaviorally relevant stimuli after damage to the right temporo-parietal junction (Cerebral Cortex)

Radek Ptak and Elena Pedrazzini

Corresponding author: Radek Ptak

Email: radek.ptak@unige.ch

This PDF file includes:

Supplementary Table 1

Supplementary Figures 1 to 3

Supplementary Table 1. Percent damage of patients with left (LH) or right (RH) hemispheric lesions in regions of interest (ROIs) of the Harvard-Oxford anatomical atlas. In order to increase clarity of this table, ROIs covering the same anatomical structure (e.g., the anterior and posterior divisions of the Middle temporal gyrus) have been merged into a single line.

		LH-damage		RH-damage	
Atlas ROI		**LH-ROI**	**RH-ROI**	**LH-ROI**	**RH-ROI**
Frontal	Frontal pole	0.03	0	0	2.04
	Superior frontal gyrus	0.27	0	0	2.85
	Middle frontal gyrus	0.27	0	0	13.83
	Inferior frontal gyrus	0.44	0	0	22.55
	Precentral gyrus	3.92	0	0	15.75
	Supplementary motor cortex	0.02	0	0	0.63
	Frontal operculum	0.19	0	0	25.50
	Frontal orbital cortex	0	0	0	6.62
	Insula	3.49	0	0	29.19
Temporal	Temporal pole	0	0	0	9.65
	Superior temporal gyrus	0.95	0	0	22.20
	Middle temporal gyrus	2	0	0	17.38
	Inferior temporal gyrus	0.07	0	0	6.45
	Planum temporale	1.98	0	0	26.95
	Heschl's gyrus	5.41	0	0	34.75
	Parahippocampal gyrus	0	0	0	2.74
	Lingual gyrus	0	0	0	2.22
	Fusiform gyrus	0	0	0	3.80
	Hippocampus	0	0	0	6.21
Parietal	Postcentral gyrus	8.49	0	0	18.04
	Superior parietal lobule	24.90	0	0	14.91
	Supramarginal gyrus	5.24	0	0	24.72
	Angular gyrus	19.41	0	0	23.57
	Parietal operculum	3.19	0	0	32.92
	Precuneus	4.07	0	0	0.86
	Cuneal cortex	9.31	0	0	1.81
Occipital	Lateral occipital cortex	17.59	0	0	11.86
	Intracalcarine cortex	0.09	0	0	3.03
	Supracalcarine cortex	1.16	0	0	2.41
	Occipital pole	7.84	0	0	5.57
Subcortical	Thalamus	0.67	0	0	4.65
	Caudate	1.42	0	0	10.46
	Putamen	2.44	0	0	21.75
	Pallidum	1.78	0	0	14.57

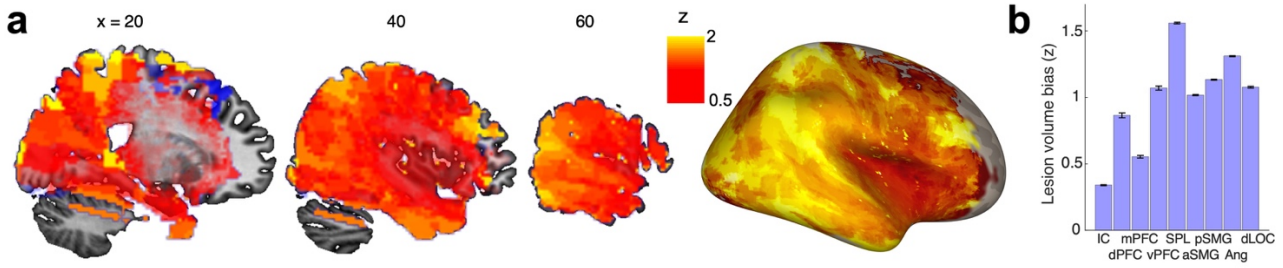

Supplementary Figure 1. Volume bias plot. a, Sagittal sections showing for each voxel color-rendered average z-scores reflecting the probability that damage is associated with lesion volume (reddish colors: voxels associated with relatively small lesions; yellowish colors: voxels associated with relatively large lesions). b, Average lesion volume bias of nine regions of interest. Abbreviations: IC: insular cortex; d/m/vPFC: dorsal/mid/ventral prefrontal cortex; SPL: superior parietal lobule; a/pSMG: anterior/posterior supramarginal gyrus; Ang: angular gyrus; dLOC: dorsal lateral occipital cortex.

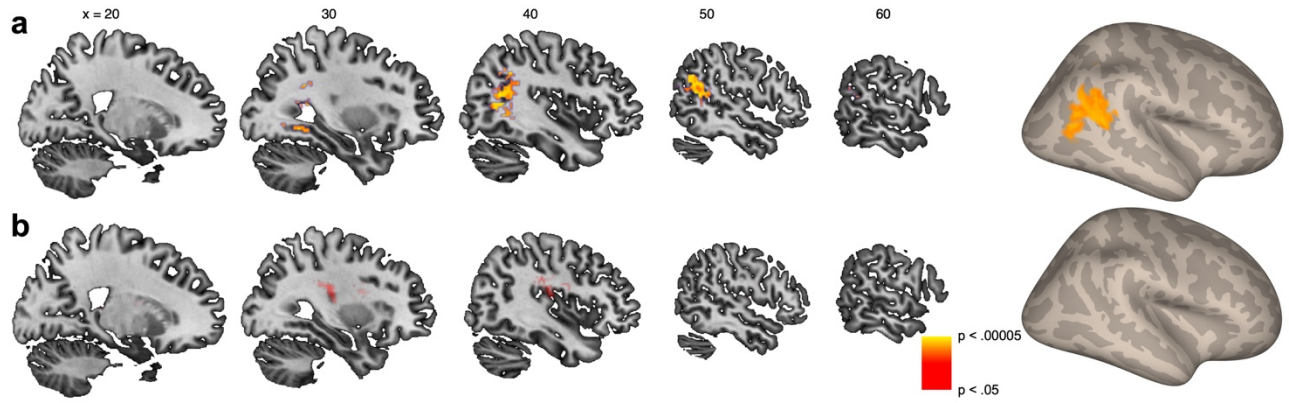

Supplementary Figure 2. SVR-LSM analyses of the validity effect. a, Sagittal sections of the template brain showing voxels whose damage predicts increased validity effects with relevant cues. **b**, Voxels associated with increased validity effects with irrelevant cues (note that the voxels presented here reached voxel-level significance $p < 0.005$, but not permutation-derived cluster-level significance). The right side shows cortical projections of these brain areas on an inflated brain. Scale shows permutation-derived cluster-level significance and x-values indicate x-location in the MNI-template.

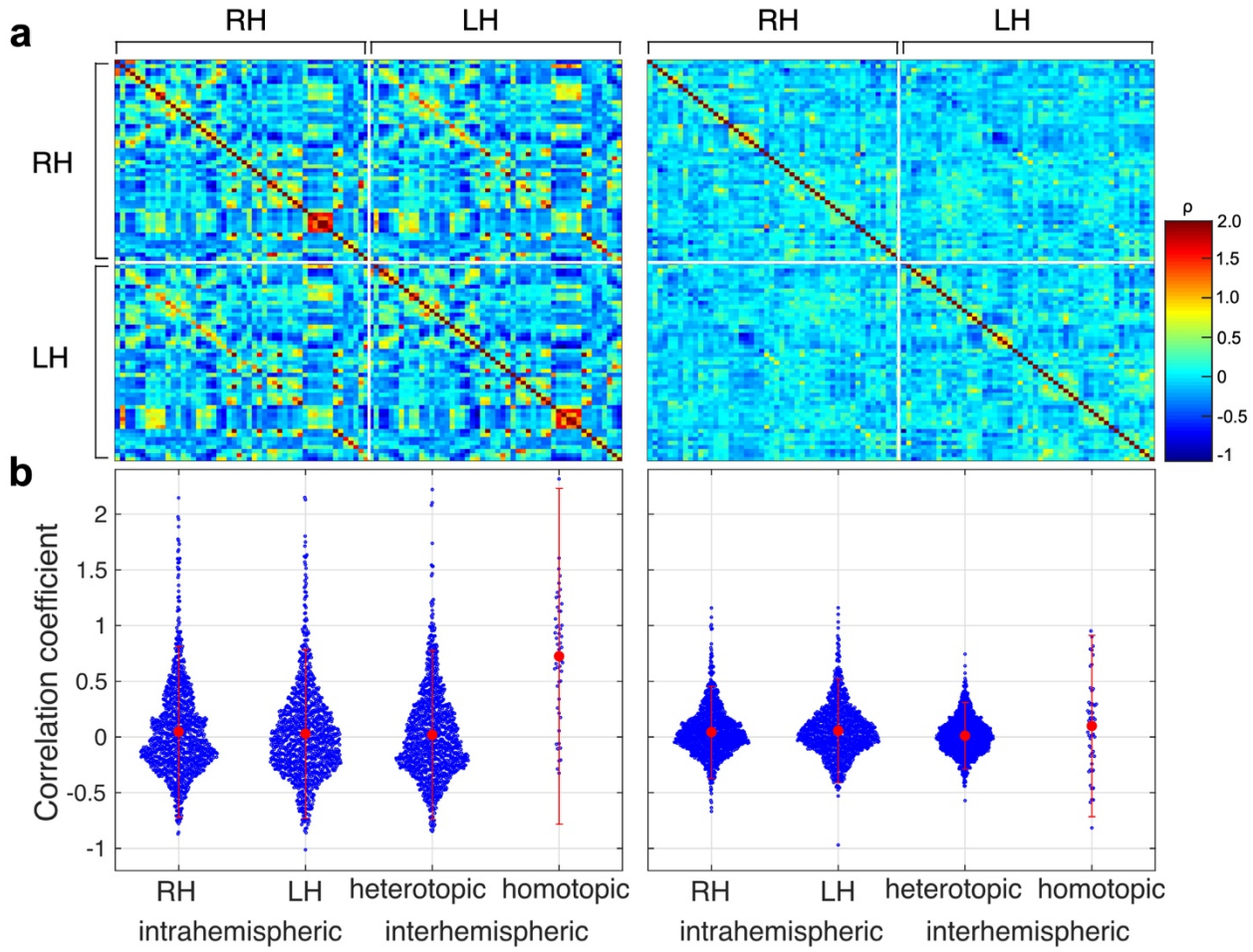

Supplementary Figure 3. Intrahemispheric and interhemispheric connectivity. **a**, Matrix of ROI-to-ROI connectivity between all 51 left- and 51 right-hemispheric ROIs. The left upper and right lower quarters show right and left intrahemispheric connectivity, respectively. The left lower and right upper quarter are identical and show interhemispheric connectivity. The color scale shows Fisher-transformed correlation coefficients (note that these coefficients can be > 1 and < -1). Left panel: healthy controls, right panel: RH-damaged patients. **b**, Bee-swarm plots of all ROI-to-ROI correlations for intrahemispheric and interhemispheric heterotopic/homotopic connectivity pairs. The red dot shows average connectivity (± 95th percentile). Left panel: healthy controls; right panel: RH-damaged patients.